JOURNAL OF AIRCRAFT
Vol. 32, No. 2, March–April 1995

Hypersonic Inviscid and Viscous Flow over a Wedge and Cone

K. K. Leung* and G. Emanuel†
University of Oklahoma, Norman, Oklahoma 73019

An analysis of hypersonic flow over a wedge and cone is developed that is based on hypersonic small-disturbance theory in combination with laminar boundary-layer theory. The parameters that determine the flow are the ratio of specific heats (= 1.4), the freestream Mach number, which ranges from 4 to 10, the wall half-angle, equal to 5, 10, or 15 deg, a wall to freestream temperature ratio, equal to 1 or 3, a Reynolds number (= 10^6), and a geometric parameter that is zero for a wedge and unity for a cone. All results are nondimensional and in a convenient form for establishing trends or for comparisons with experimental or CFD data. Results are provided for the inviscid surface values of the pressure, temperature, and Mach number; wave and viscous drag coefficients and several heat transfer coefficients; the maximum temperature and its location inside the boundary layer; and a variety of viscous and thermal boundary-layer thicknesses. The independent parameter is the freestream Mach number; the dependence on the wall to freestream temperature ratio and a Reynolds number are explicitly given.

Nomenclature

A = area
C_D = drag coefficient
c_p = specific heat at constant pressure
D = drag
f = boundary-layer stream function
g = stagnation temperature ratio, T_0/T_{0e}
K_β = hypersonic similarity parameter, $M_\infty\beta$
K_θ = hypersonic similarity parameter, $M_\infty\theta$
l = body length
M = Mach number
n = coordinate normal to the wall
Pr = Prandtl number
p = pressure
Q_W = global heat transfer parameter
q = heat transfer
q_∞ = freestream dynamic pressure, $\frac{1}{2}\gamma p_\infty M_\infty^2$
Re_l = freestream Reynolds number, $(\rho U/\mu)_\infty l$
Re_s = boundary-layer Reynolds number, $(\rho u/\mu)_e s$
$\bar{R}e_s$ = Reynolds number based on wall length, $(p_e/p_\infty)(T_\infty/T_e)^2(u_e/U_\infty)(Re_l/\cos\theta_w)$
r = radial coordinate
S = speed parameter, $[(\gamma - 1)/2]M^2/\{1 + [(\gamma - 1)/2]M^2\}$
St = Stanton number
s = coordinate along the wall measured from the apex
T = temperature
U_∞ = freestream speed
u = flow speed parallel to the wall
β = shock wave angle
γ = ratio of specific heats
δ = velocity boundary-layer thickness, equals n when $f' = 0.99$
δ_t = thermal boundary-layer thickness, equals n when $(g - g_w) = 0.99(1 - g_w)$
δ^* = displacement thickness, $\int_0^\infty [1 - (\rho u/\rho_e u_e)]\,dn$
η = similarity variable, $[(\rho u)_e r_w^\sigma/(2\xi)^{1/2}]\int_0^n (\rho/\rho_e)\,dn$
θ = velocity angle relative to the centerline
θ = momentum defect thickness, $\int_0^\infty (\rho u/\rho_e u_e)[1 - (u/u_e)]\,dn$
κ = thermal conductivity
μ = viscosity
ξ = boundary-layer wall coordinate, $(\rho\mu u)_e s(\frac{1}{3}s^2\sin^2\theta_w)^\sigma$
ρ = density
σ = 0 for a wedge, 1 for a cone
τ = shear stress
ϕ = stagnation enthalpy defect thickness, $\int_0^\infty (\rho u/\rho_e u_e)[1 - (T_0 - T_{0w})/(T_{0e} - T_{0w})]\,dn$

Subscripts

b = base
c = cone
d = conditions just downstream of the shock
e = boundary-layer edge
m = temperature maximum inside the boundary layer
v = viscous
w = wall, wedge, or wave
0 = stagnation
∞ = freestream

Superscripts

$'$ = derivative with respect to η
$\bar{}$ = indicates s is replaced with $l\sec\theta_w$

Introduction

HYPERSONIC flow over simple shapes has been of interest for some time.[1,2] Previous studies often focus on a specific application or phenomenon such as viscous interaction. There is thus a need for a simple inviscid/viscous treatment of flow properties and parameters associated with hypersonic flow over a wedge and cone at zero incidence. Our objective is to provide trends in a convenient format for comparison or correlation with experiment or other theoretical/computational studies. Thus, the direction of a trend can be assessed, and the possible need to incorporate additional factors, e.g., base drag, established. Moreover, this approach can be the starting point for more elaborate analysis. For example, the maximum temperature formulation can be used to assess the onset of vibrational relaxation, air dissociation, or radiative heat transfer.

Hypersonic small-disturbance theory (HSDT) is combined with a laminar boundary-layer analysis. The analysis assumes a nonreacting perfect gas with no radiative heat transfer. The freestream Mach number M_∞ and cone or wedge half angle

Received May 3, 1994; revision received July 18, 1994; accepted for publication July 18, 1994.

*Graduate Student, School of Aerospace and Mechanical Engineering. Student Member AIAA.
†Professor, School of Aerospace and Mechanical Engineering. Associate Member AIAA.

θ_w, satisfy the hypersonic small disturbance requirement that K_θ is of order unity. Hence, the bow shock is attached and viscous interaction is neglected. For the boundary layer, the wall is assumed to have a constant temperature, and the Prandtl number and Chapman-Rubesin parameter are unity.[3]

Nondimensional results are determined by γ, M_∞, θ_w, T_w/T_∞, σ, and Re_l. For these parameters we take $\gamma = 1.4$, $4 \leq M_\infty \leq 10$, $\theta_w = 5, 10, 15$ deg, $T_w/T_\infty = 1, 3$, and $Re_l = 10^6$. The upper limit on M_∞ stems from the neglect of viscous interaction, real gas effects, and radiative heat transfer. When $M_\infty = 10$ some of these effects may start to become significant. The ranges chosen for M_∞ and θ_w yield $0.349 \leq K_\theta \leq 2.62$, which is a nominal range for hypersonic flight. The temperature ratios of 1 and 3 are, respectively, for cold and hot wall surfaces. One Reynolds number value is sufficient, since those quantities that depend on it scale as $Re_l^{\ 1/2}$. Moreover, for a sharp cone or wedge with a smooth surface in free flight, the laminar regime corresponds to a Reynolds number well in excess of 10^6 (Refs. 4 and 5).

Results are presented in four categories. The first provides inviscid surface conditions for the pressure, temperature, and Mach number. The next group consists of wave and viscous drag coefficients and two heat transfer coefficients. Base drag is not included, i.e., the base pressure is assumed equal to p_∞. One heat transfer coefficient is the local Stanton number, whereas the second coefficient is the global heat transfer that is conveniently normalized in a manner similar to the drag coefficients. The third group provides the maximum temperature inside the boundary layer and its location in both the transformed and physical planes. The last group contains results for commonly encountered viscous and thermal thicknesses. These include the velocity, thermal, displacement, momentum defect, and stagnation enthalpy defect thicknesses.

In line with the above goals, it is more convenient to use M_∞ as the principle independent parameter rather than K_θ. This choice is partly motivated by the dominance of viscous results for which M_∞ is an appropriate choice. Thus, result figures contain six curves, three for the wedge and three for the cone, where the curves correspond to the different θ_w values. Hence, for a given parameter, more than one figure is required only when T_w/T_∞ is significant. Further details and results can be found in the thesis[6] on which this article is based.

Formulation

For purposes of clarity, we succinctly summarize the HSDT and boundary-layer equations. The shock wave angle β (see Fig. 1) and velocity turn angle θ_d are related by

$$\tan(\beta - \theta_d) = \frac{2}{\gamma + 1} \frac{1 + [(\gamma - 1)/2]M_\infty^2 \sin^2\beta}{M_\infty^2 \sin\beta \cos\beta}$$

With the introduction of the HSDT limit, we have

$$K_\beta - K_{\theta_d} = \frac{2}{\gamma + 1} \frac{1 + [(\gamma - 1)/2]K_\beta^2}{K_\beta}$$

In the wedge case, the inviscid flow between the shock and wedge is uniform and θ_d is replaced with $\theta\ (= \theta_w)$, with the result

$$K_{\beta w} = \frac{\gamma + 1}{4} K_\theta + \left[1 + \left(\frac{\gamma + 1}{4} K_\theta\right)^2\right]^{1/2}$$

In the cone case, $\theta_d \neq \theta_w$, and the approximation[7]

$$K_{\beta c} = \{1 + [(\gamma + 1)/2]K_\theta^2\}^{1/2}$$

is utilized, where again $\theta = \theta_w$.

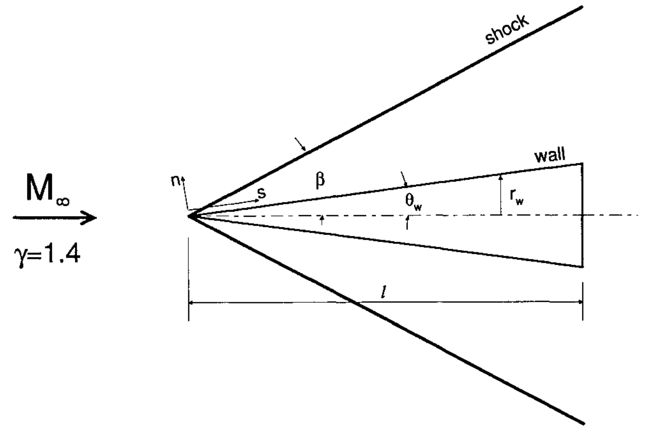

Fig. 1 Schematic for flow over a wedge or cone.

For the wedge, it is sufficient to write the exact planar shock jump conditions and apply HSDT to directly obtain

$$\frac{p_e}{p_\infty} = \frac{2}{\gamma + 1}\left(\gamma K_{\beta w}^2 - \frac{\gamma - 1}{2}\right)$$

$$\frac{T_e}{T_\infty} = \frac{2}{\gamma + 1} \frac{1 + [(\gamma - 1)/2]K_{\beta w}^2}{K_{\beta w}^2} \frac{p_e}{p_\infty}$$

$$M_e = \frac{M_\infty}{K_{\beta w} - K_\theta}\left\{\frac{1 + [(\gamma - 1)/2]K_{\beta w}^2}{\gamma K_{\beta w}^2 - [(\gamma - 1)/2]}\right\}^{1/2}$$

$$\frac{u_e}{U_\infty} = \frac{M_e}{M_\infty}\left(\frac{T_e}{T_\infty}\right)^{1/2}$$

Similar HSDT results for the cone[8] are

$$\frac{p_e}{p_\infty} = 1 + \gamma K_\theta^2 \left\{\frac{1}{2} + \frac{1 + [(\gamma + 1)/2]K_\theta^2}{1 + [(\gamma - 1)/2]K_\theta^2} \ln\left(\frac{K_{\beta c}}{K_\theta}\right)\right\}$$

$$\frac{T_e}{T_\infty} = 1 + (\gamma - 1)K_\theta^2 \left[\frac{1}{2} + \ln\left(\frac{K_{\beta c}}{K_\theta}\right)\right]$$

$$\frac{u_e}{U_\infty} = 1 - \theta_w^2\left[\frac{1}{2} + \ln\left(\frac{K_{\beta c}}{K_\theta}\right)\right], \qquad M_e = M_\infty \left(\frac{T_\infty}{T_e}\right)^{1/2} \frac{u_e}{U_\infty}$$

Table 1 compares HSDT and exact results just downstream of the shock and on the surface. Two cases are shown, both have $K_\theta = 1.047$, where the exact results for the cone stem from Sims.[9] Agreement between HSDT and the exact results is excellent. The largest error is in the M_e (or M_d) wedge value when $M_\infty = 4$, where the error is -10%. This error does not extend to the other $M_\infty = 4$ wedge values, e.g., the p_e/p_∞ (or p_d/p_∞) value is in error by only 1%. Moreover, it does not extend to the $M_\infty = 4$ cone case, where the error in M_e is only 0.6%. The error in M_e for a wedge rapidly decreases with M_∞; it is only -4% at $M_\infty = 6$.

In line with the earlier discussion, the boundary-layer pressure gradient parameter is zero and a similar solution is assumed. We thus have the Blasius equation

$$f''' + ff'' = 0, \qquad f_w = f'_w = 0, \qquad f'(\infty) = 1 \qquad (1)$$

where $(u/u_e) = df/d\eta = f'$. The solution of the energy equation is

$$(g - g_w)/(1 - g_w) = f'$$

Table 1 Comparison of exact and HSDT solutions just downstream of the shock and on the surface for a wedge and a cone

	$M_\infty = 4$, $\theta_w = 15$ deg				$M_\infty = 6$, $\theta_w = 10$ deg			
	Wedge		Cone		Wedge		Cone	
	Exact	HSDT	Exact	HSDT	Exact	HSDT	Exact	HSDT
β, deg	27.06	25.92	21.79	21.80	17.59	17.28	14.35	14.53
M_d	2.929	3.225	3.321	3.286	4.648	4.837	5.124	5.074
M_e	2.929	3.225	3.217	3.197	4.648	4.837	4.993	4.966
p_d/p_∞	3.697	3.653	2.406	2.535	3.668	3.653	2.414	2.535
p_e/p_∞	3.697	3.653	2.801	2.858	3.668	3.653	2.810	2.858
T_d/T_∞	1.547	1.539	1.310	1.335	1.541	1.539	1.312	1.335
T_e/T_∞	1.547	1.539	1.368	1.383	1.541	1.539	1.370	1.383

which yields the quadratic[3] in u/u_e

$$\frac{T}{T_w} = \frac{\rho_w}{\rho} = 1 + \frac{1 - g_w}{g_w} f' - \frac{S_e}{g_w} f'^2 \qquad (2)$$

where

$$g_w = T_w/T_{0e} = (1 - S_\infty)(T_w/T_\infty)$$

The various boundary-layer thicknesses mentioned earlier can be written nondimensionally as[3]

$$\frac{\delta}{s} = \frac{\delta_t}{s} = \left[\frac{2}{(2\sigma + 1)Re_s}\right]^{1/2} \left(\eta_{ev} - C_v + \frac{f''_w S_e + C_v g_w}{1 - S_e}\right)$$

$$\frac{\delta^*}{s} = \left[\frac{2}{(2\sigma + 1)Re_s}\right]^{1/2} \left(\frac{f''_w S_e + C_v g_w}{1 - S_e}\right)$$

$$\frac{\theta}{s} = \frac{\phi}{s} = \left[\frac{2}{(2\sigma + 1)Re_s}\right]^{1/2} f''_w$$

where the constants are $f''_w = 0.4696$, $\eta_{ev} = 3.4717$, and $C_v = 1.2168$.

Results

Figures 2–4 show inviscid surface results for the pressure, temperature, and Mach number. The barely discernible crossover in the $\theta_w = 15$-deg curves near $M_\infty = 5$ in Fig. 4 should be disregarded. It is caused by the $M_\infty = 4$ error previously discussed. The pressure and temperature values are larger for the wedge than for the cone, where the opposite trend holds for M_e. For given values of M_∞ and θ_w, the shock is weaker for the cone (e.g., see β in Table 1), but there is a further compression as a streamline approaches the cone's surface. As a consequence of these two effects, M_e differs only slightly between the wedge and cone.

The drag coefficients are normalized with the base area

$$A_b = 2l \tan \theta_w[(\pi/2)l \tan \theta_w]^\sigma$$

The wave and viscous drags are

$$D_w = (p_e - p_\infty)A_b$$

$$D_v = \cos \theta_w \int_0^{\bar{A}_w} \tau_w \, dA$$

where A_w is the surface area from the apex to s

$$A_w = 2s[(\pi/2)s \sin \theta_2]^\sigma$$

and the wetted surface area $\bar{A}_w$ is its value when $s = l \sec \theta_w$. We thus obtain

$$D_v = 2^{3/2}(\rho u^2)_e \left(\frac{\pi}{3^{1/2}} l \tan \theta_w\right)^\sigma \frac{l f''_w}{\bar{R}e_w^{1/2}}$$

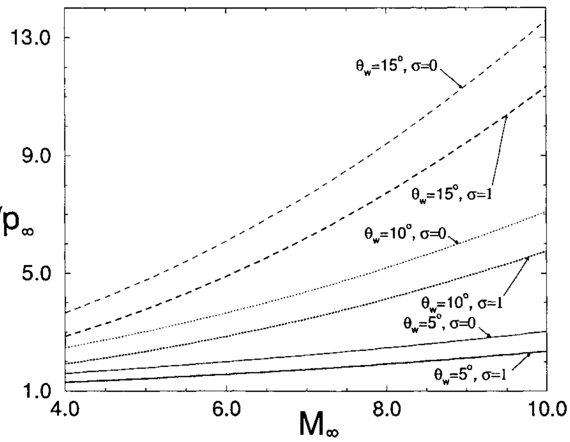

Fig. 2 Inviscid surface pressure as a function of M_∞.

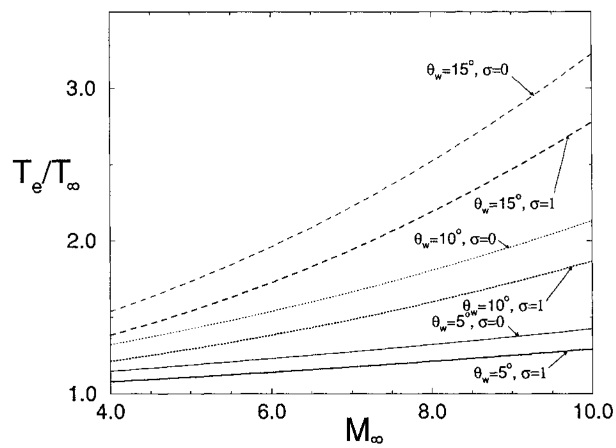

Fig. 3 Inviscid surface temperature as a function of M_∞.

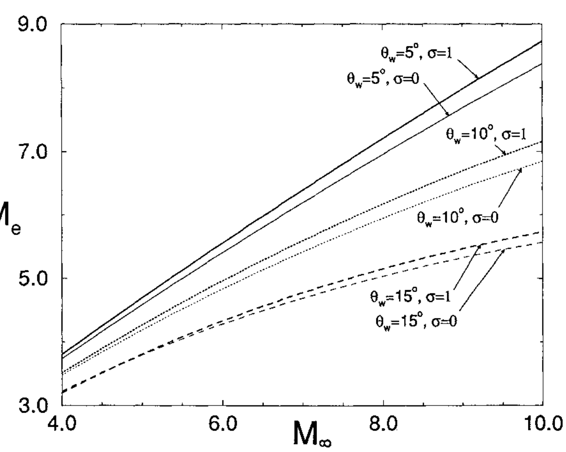

Fig. 4 Inviscid surface Mach number as a function of M_∞.

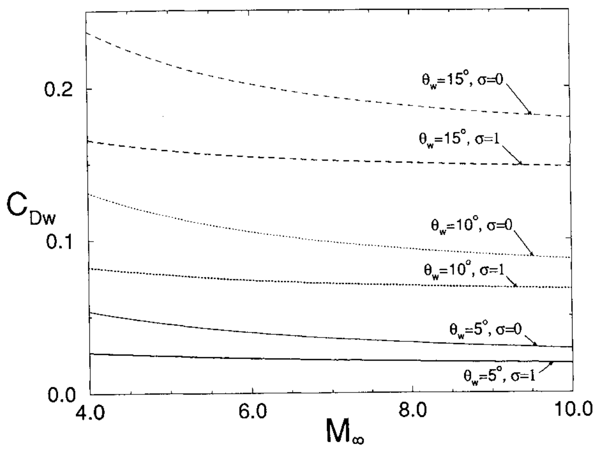

Fig. 5 Global wave drag coefficient as a function of M_∞.

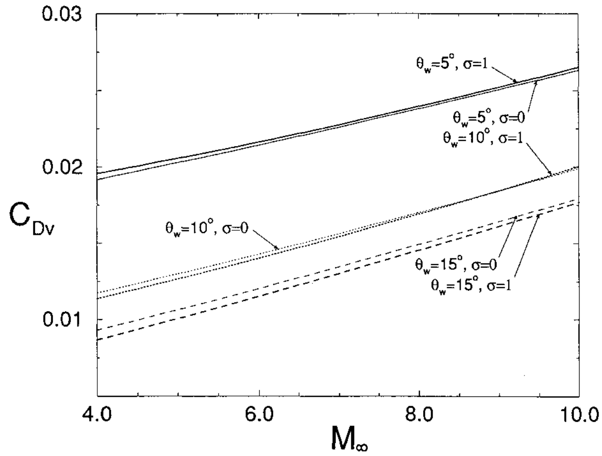

Fig. 6 Global viscous drag coefficient as a function of M_∞.

where $\bar{Re}_s$ (see nomenclature) is proportional to Re_l. The drag coefficients thus become

$$C_{Dw} = \frac{D_w}{q_\infty A_b} = \frac{2}{\gamma M_\infty^2}\left(\frac{p_e}{p_\infty} - 1\right)$$

$$C_{Dv} = \frac{D_v}{q_\infty A_b} = \frac{2^{3/2+\sigma}}{3^{\sigma/2}}\frac{p_e}{p_\infty}\frac{T_\infty}{T_e}\left(\frac{u_e}{U_\infty}\right)^2 \frac{f''_w}{\bar{Re}_s^{1/2}\tan\theta_w} \tag{3}$$

where $C_{Dw} + C_{Dv}$ is the total drag coefficient associated with the wetted surface area. Ratios such as p_e/p_∞ and T_e/T_∞ are provided by the HSDT formulas of the preceding section.

Figure 5 shows that the wave drag coefficient is nearly independent of M_∞, particularly for a slender body. Hence, D_w is roughly proportional to M_∞^2. As indicated in Fig. 6, there is little difference between the wedge and cone C_{Dv} values. Although both coefficients are normalized with A_b, C_{Dw} increases with θ_w, whereas C_{Dv} has the opposite trend. The shock strengthens with θ_w, which causes C_{Dw} to increase. On the other hand, the tan θ_w factor in Eq. (3) is responsible for the C_{Dv} trend. A comparison of Figs. 5 and 6 shows the dominance of the wave drag, except when θ_w is small. Of course, any such comparison also depends on the value of Re_l.

The heat transfer is written as

$$q_w = -\kappa_w\left(\frac{\partial T}{\partial n}\right)_w = -\left(\frac{2\sigma+1}{2}Re_s\right)^{1/2}\frac{c_p u_e T_w}{s}\left(\frac{1-g_w}{g_w}\right)f''_w$$

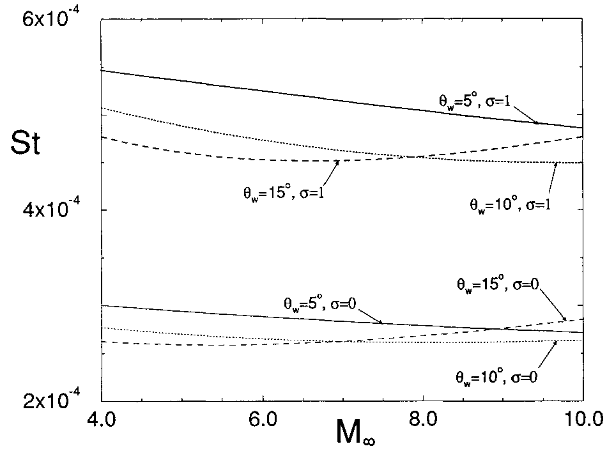

Fig. 7 Local Stanton number as a function of M_∞.

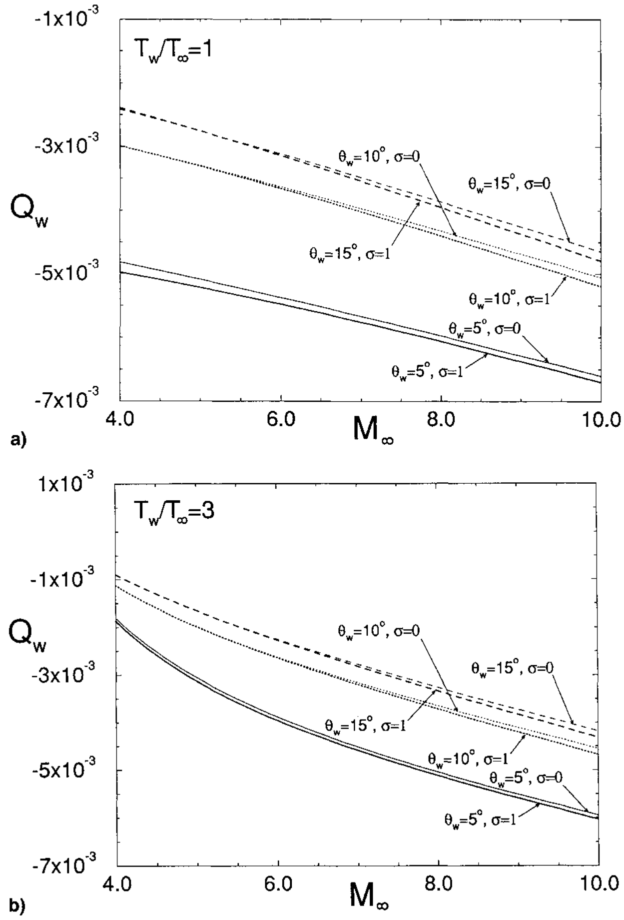

Fig. 8 Global heat transfer coefficient as a function of M_∞; T_w/T_∞ = a) 1 and b) 3.

and the local Stanton number is

$$St = \frac{q_w}{c_p(T_{0w} - T_{0e})(\rho u)_e} = \frac{3^{\sigma/2}f''_w}{(2Re_s)^{1/2}} \tag{4}$$

The connection between any local quantity with a $Re_s^{-1/2}$ dependence and its global counterpart is given by

$$\frac{1}{A_b}\int_0^{A_w}\frac{dA_w}{Re_s^{1/2}} = 2\left(\frac{2}{3}\right)^\sigma \frac{T_e}{T_\infty}\left(\frac{p_\infty}{p_e}\frac{U_\infty}{u_e}\right)^{1/2}\frac{1}{\bar{Re}_s^{1/2}\sin\theta_w} \tag{5}$$

Figure 7 shows the curves for the Stanton number in two groups because of the $3^{\sigma/2}$ factor. Within each group the curves are proportional to $Re_s^{-1/2}$ and are only weakly dependent on M_∞. A Prandtl number correction can be introduced with Colburn's analogy[3] by multiplying the right side of Eq. (4) with $Pr^{-2/3}$. Thus, the Stanton number values in Fig. 7 should be increased by about 25% for air.

A more convenient heat transfer parameter would be global and normalized in a manner similar to the drag coefficients. We thus introduce

$$Q_W = \frac{1}{(\rho U^3)_\infty A_b} \int_0^{A_w} q_w \, \mathrm{d}A_w$$

$$= -\frac{2^{\sigma - 1/2}}{3^{\sigma/2}} \frac{p_e}{p_\infty} \frac{T_\infty}{T_e} \frac{u_e}{U_\infty} \frac{(1 - g_w) f''_w}{S_\infty \tilde{R}e_s^{1/2} \sin \theta_w}$$

where Eq. (5) is utilized. Figure 8 shows Q_W for $(T_W/T_\infty) =$ 1 and 3, where Q_W is negative when the heat transfer is into the wall. The figures show a weak dependence on σ, but a steadily increasing value for $|Q_w|$ with M_∞.

At hypersonic speeds, a constant wall temperature boundary layer with $1 > g_w$ has a significant temperature overshoot, which is caused by viscous dissipation. The peak temperature T_m and its location η_m are obtained as

$$\frac{T_m}{T_w} = 1 + \frac{(1 - g_w)^2}{4 g_w S_e} \tag{6a}$$

$$f'(\eta_m) = \frac{1 - g_w}{2 S_e} \tag{6b}$$

by differentiating Eq. (2) with respect to η. The general inversion of the η integral definition is given in Ref. 3. For the problem at hand, this yields

$$\frac{n_m}{s} = \frac{1}{1 - S_e} \left[\frac{2}{(2\sigma + 1) Re_s} \right]^{1/2} \{ g_w \eta_m + (1 - g_w) f(\eta_m)$$
$$- S_e [f''(\eta_m) + f(\eta_m) f'(\eta_m) - f''_w] \}$$

where η_m is determined by Eq. (6b), and an accurate solution of Eqs. (1) yields $f(\eta_m)$, $f'(\eta_m)$, and $f''(\eta_m)$. The above equation shows that $n_m \sim s^{1/2}$. From Eq. (6a), the peak temperature becomes infinite when $g_w \to 0$.

Figure 9 shows that T_m/T_∞ is barely altered by either σ or θ_w, which is in sharp contrast to the inviscid result of Fig. 3. There is a strong dependence on T_w/T_∞, and on M_∞, which is caused by viscous dissipation heat production. Figure 10 shows η_m for $(T_w/T_\infty) = 1$ and 3. When $(T_w/T_\infty) = 1$, η_m is between 1.1–1.25 and has a weak dependence on M_∞. The curves are quite different when $(T_w/T_\infty) = 3$, where they increase rapidly with M_∞, especially when M_∞ is relatively small. The location of T_m in the physical plane is shown in Fig. 11, where we observe that n_m is larger for a wedge than for a cone. The corresponding difference is much less for η_m. Also evident is that the location of the peak temperature is closest to the wall when θ_w is large and $\sigma = 1$. This conclusion is in accord with the earlier Stanton number result.

Results are given for three boundary-layer thicknesses, since $\delta_t = \delta$ and $\phi = \theta$ with the current assumptions. Curves for δ/s are shown in Fig. 12, where the wedge has the larger boundary-layer thickness. Displacement thickness results are shown in Fig. 13. Although the magnitude of δ^* is substantially less than δ, the trends are similar. Figure 14 shows the momentum thickness whose magnitude is well below that of

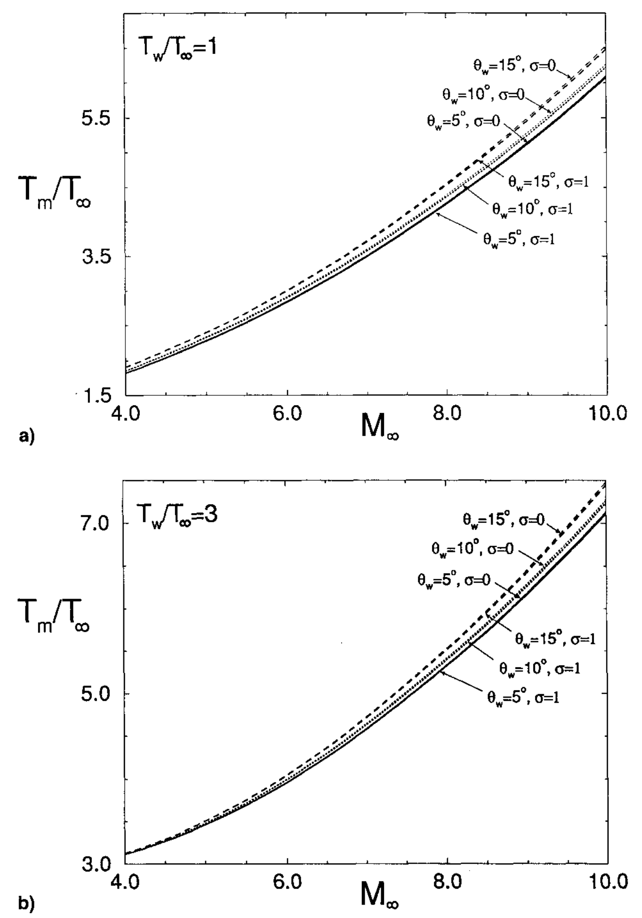

Fig. 9 Maximum temperature inside the boundary layer as a function of M_∞; T_w/T_∞ = a) 1 and b) 3.

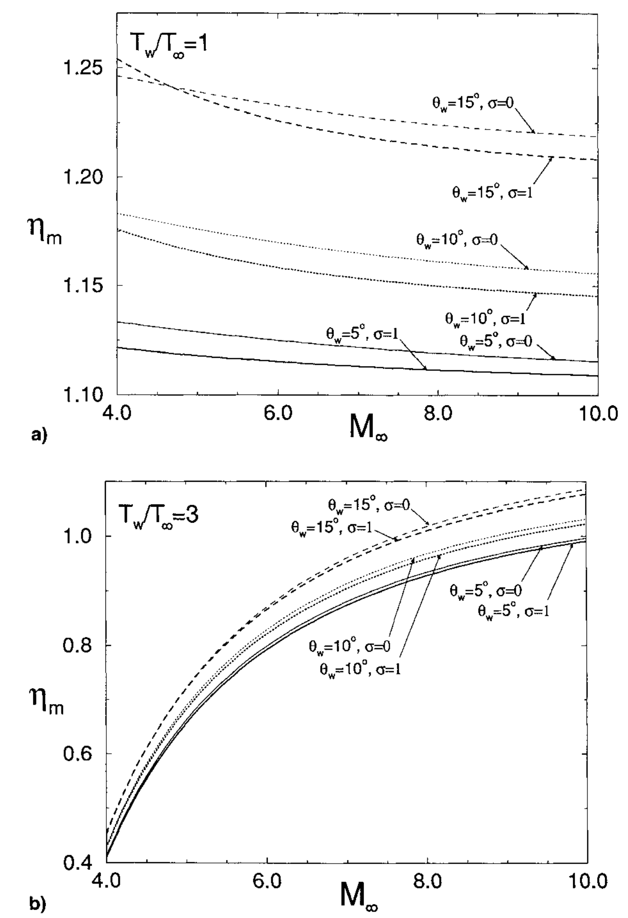

Fig. 10 Transformed coordinate η_m as a function of M_∞; T_w/T_∞ = a) 1 and b) 3.

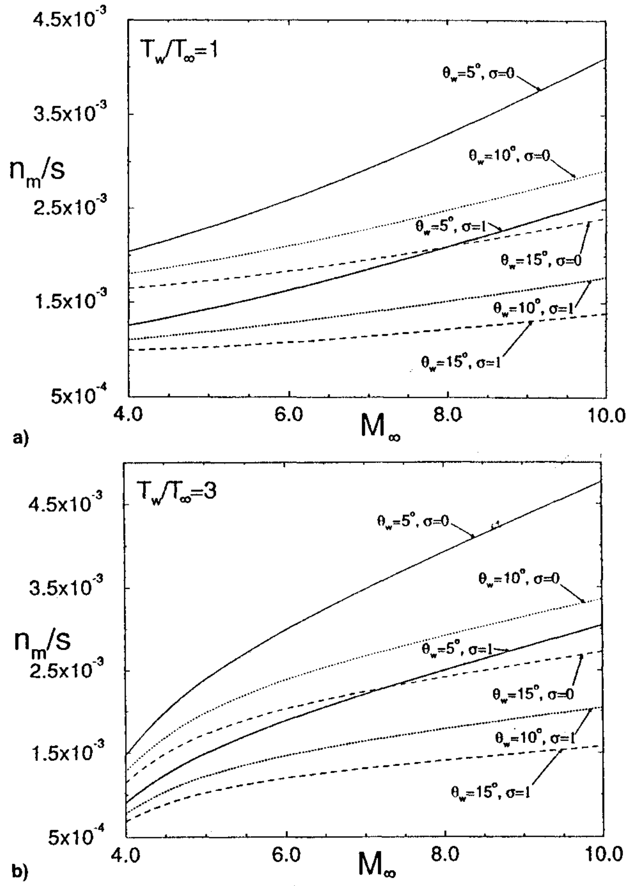

Fig. 11 Physical coordinate n_m as a function of M_∞; T_w/T_∞ = a) 1 and b) 3.

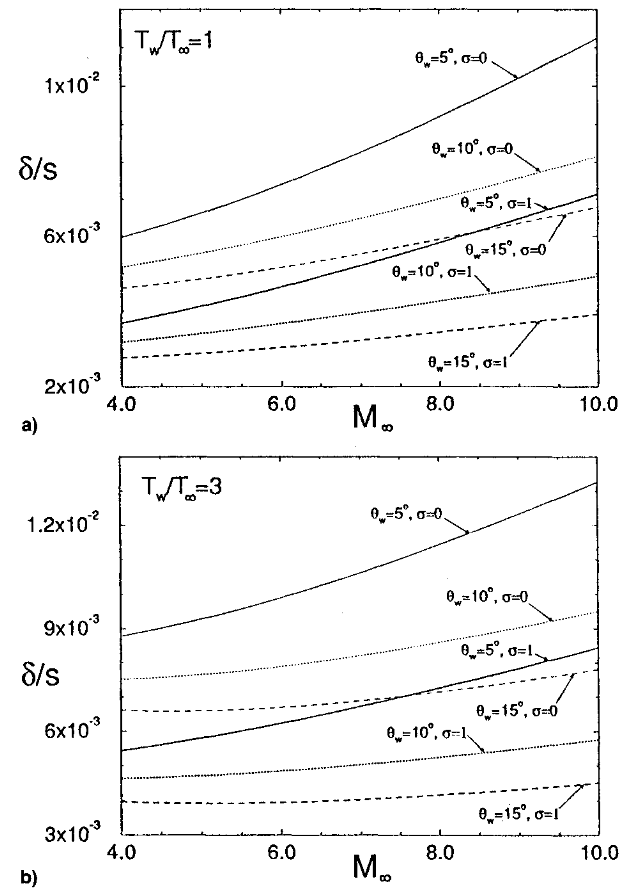

Fig. 12 Velocity and thermal thicknesses as a function of M_∞; T_w/T_∞ = a) 1 and b) 3.

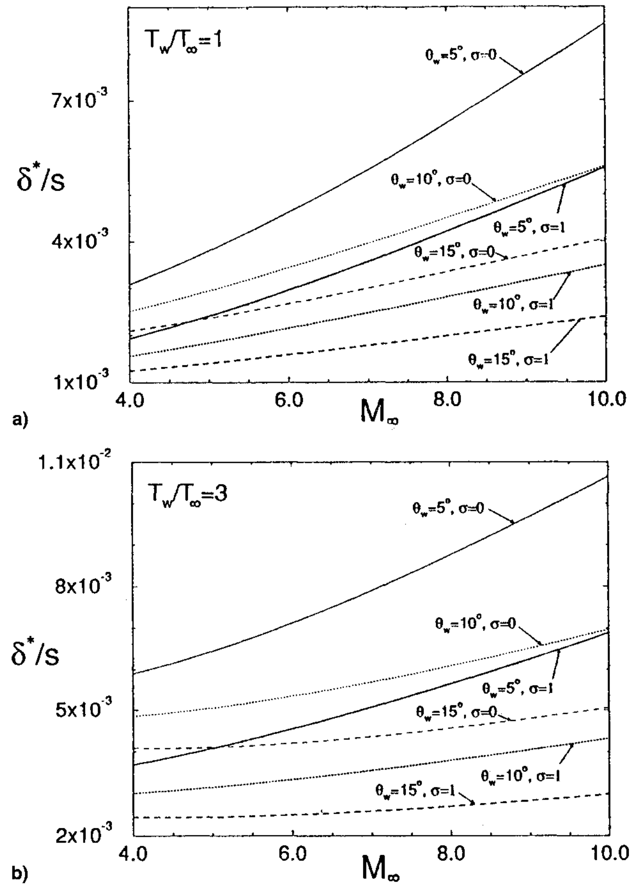

Fig. 13 Displacement thickness as a function of M_∞; T_w/T_∞ = a) 1 and b) 3.

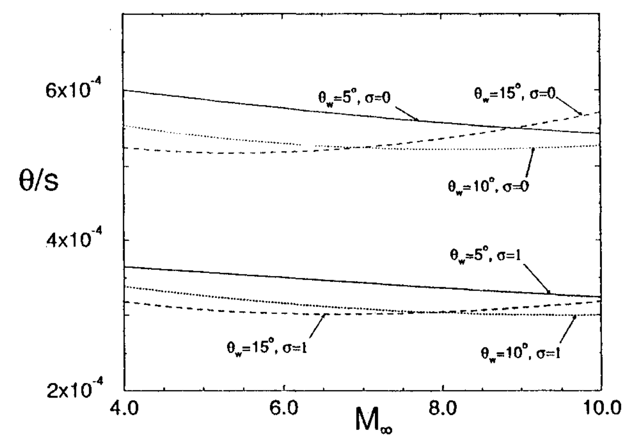

Fig. 14 Momentum defect and stagnation enthalpy defect thicknesses as a function of M_∞.

δ^*. Moreover, there is no dependence on T_w/T_∞, little dependence on M_∞, and the wedge and cone values are segregated.

Concluding Remarks

A parametric treatment is provided for hypersonic flow over a wedge and a cone at zero angle of attack. The analysis combines hypersonic small-disturbance theory with laminar boundary-layer theory. Results are grouped into four categories. In the first, inviscid surface values for the pressure, temperature, and Mach number are given. The second category encompasses wave and skin friction drag coefficients and two heat transfer parameters. The third category provides the maximum temperature and its location within the boundary layer. The final group provides a variety of viscous and thermal boundary-layer thicknesses. All results are nondimensional and are in a convenient form for establishing trends and correlating experimental or CFD data.

An important extension of the analysis occurs when the upstream flow is nonuniform but still parallel to the centerline or symmetry axis. With a cone, the flow must still be axisymmetric. Thus, the flow upstream and downstream of the bow shock is vortical and possesses a transverse gradient of the stagnation enthalpy and/or of the entropy. This vortical flow can be analyzed in terms of the previously given inviscid results using the substitution principle.[3] External vorticity and a transverse gradient of entropy or stagnation enthalpy alter the skin friction, heat transfer, boundary-layer thicknesses, etc. The resultant change in viscous properties can be assessed with second-order boundary-layer theory,[3] which would also assess the effect of displacement and transverse curvature.

References

[1]Chernyi, G. G., *Introduction to Hypersonic Flow*, Academic Press, New York, 1961, pp. 79–94.

[2]Probstein, R. F., and Hayes, W. D., *Hypersonic Flow Theory*, Academic, New York, 1966, pp. 139–150.

[3]Emanuel, G., *Analytical Fluid Dynamics*, CRC Press, Boca Raton, FL, 1994, pp. 251–288, Chaps. 8 and 18.

[4]Sternberg, J., "A Free-Flight Investigation of the Possibility of High Reynolds Number Supersonic Laminar Boundary Layers," *Journal of the Aeronautical Sciences*, Vol. 19, No. 11, 1952, pp. 721–733.

[5]Pate, S. R., "Measurements and Correlations of Transition Reynolds Numbers on Sharp Slender Cones at High Speeds," *AIAA Journal*, Vol. 9, No. 6, 1971, pp. 1082–1090.

[6]Leung, K. K., "Flow Properties About a Cone and Wedge in Hypersonic Flow," M.S. Thesis, Univ. of Oklahoma, Norman, OK, 1993.

[7]Kim, B. S., Rasmussen, M. L., and Jischke, M. C., "Optimization of Waverider Configurations Generated from Axisymmetric Conical Flows," *Journal of Spacecraft and Rockets*, Vol. 20, No. 5, 1983, pp. 461–469.

[8]Rasmussen, M. L., and He, X., "Analysis of Cone-Derived Waveriders by Hypersonic Small-Disturbance Theory," First International Hypersonic Waverider Symposium, Univ. of Maryland, College Park, MD, Oct. 1990.

[9]Sims, J. L., "Tables for Supersonic Flow Around Right Circular Cones at Zero Angle of Attack," G. C. Marshall Space Flight Center, NASA SP-3004, 1964.